IEEE Photonics Journal
An IEEE Photonics Society Publication

Open Access

Color Tuning and White Light by Dispersing CdSe, CdTe, and CdS in PMMA Nanocomposite Waveguides

Volume 5, Number 2, April 2013

H. Gordillo
I. Suárez
R. Abargues
P. Rodríguez-Cantó
J. P. Martínez-Pastor

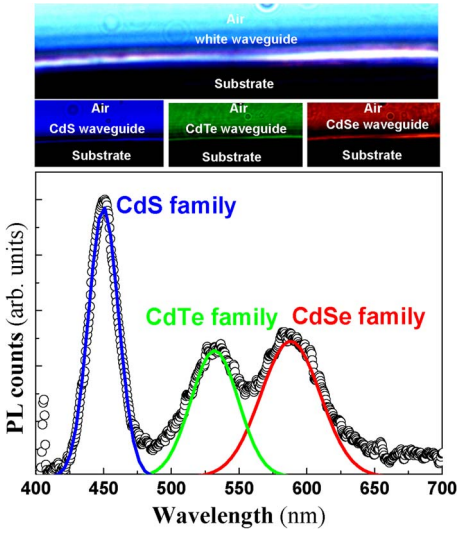

DOI: 10.1109/JPHOT.2013.2257713
1943-0655/$31.00 ©2013 IEEE

IEEE photonics SOCIETY

IEEE

Color Tuning and White Light by Dispersing CdSe, CdTe, and CdS in PMMA Nanocomposite Waveguides

H. Gordillo, I. Suárez, R. Abargues, P. Rodríguez-Cantó, and J. P. Martínez-Pastor

UMDO (Unidad Asociada al CSIC-IMM), Instituto de Ciencia de los Materiales, Universidad de Valencia, 46071 Valencia, Spain

DOI: 10.1109/JPHOT.2013.2257713
1943-0655/$31.00 ©2013 IEEE

Manuscript received March 20, 2013; revised April 4, 2013; accepted April 4, 2013. Date of publication April 15, 2013; date of current version April 18, 2013. This work was supported in part by the Generalitat Valenciana under Grant PROMETEO/2009/074, by the Spanish MINECO under Grant TEC2011-29120-C05-01, and by the EU-NAVOLCHI under Grant 288869. Corresponding author: I. Suárez (e-mail: isaac.suarez@uv.es).

Abstract: In this paper, active nanocomposite waveguides based on the dispersion of CdS, CdTe, and CdSe colloidal quantum dots (QDs) in PMMA are proposed. Their propagation properties are studied as a function of the concentration of nanoparticles in the polymer using the variable length stripe method. When the three nanostructures are dispersed in the same film, the structure is able to waveguide the three basic colors: red (CdSe), green (CdTe), and blue (CdS), it being possible to engineer any waveguided color by an appropriate choice of the filling factor of each QD in the PMMA matrix. For this purpose, it is important to take into account reabsorption effects and the Förster energy transfer between the different QDs families. As a final application, white waveguided light at the output of the structure is demonstrated. This energy transfer can be also the origin of the surprising observation that initial gain (losses) are much higher (smaller) in these active multinanopaticle waveguides than in single-loaded ones.

Index Terms: Photonic materials, colloidal quantum dots (QDs), optical waveguides, display materials.

1. Introduction

Nowadays, there is a great concern in the integration of active materials into a silicon-based technology in order to provide active functions into a photonic device. For this purpose, the choice of colloidal quantum dots (QDs) seems to be an interesting option as a material able to efficiently generate light [1]. These QDs are semiconductor nanoparticles synthesized by colloidal chemistry. Then, a 3-D confinement of the carriers is observed by the accurate control of the nanoparticle radius from 1 to 10 nm during the synthesis [2]. As a consequence, quantum size confinement is observed with a tunable effective band gap depending on size and base material. For example, spontaneous emission from red to blue has been demonstrated using CdSe [3] and CdS [4]. Besides, CdSe was used to demonstrate lasing in the red, blue, and green using QDs of different sizes [5].

In order to integrate colloidal QDs in photonic devices, a direct approach is to embed the nanostructures into a solid state matrix [7]. This kind of synthetic material, so-called nanocomposite, has the advantage of joining the properties of the QDs with those provided by the matrix, which can be selected depending on requirements of the device technology. Waveguides based on the incorporation of CdSe QDs into the solid state matrix were implemented to demonstrate amplification

of the spontaneous emission [7]. These kinds of matrices exhibit the advantages of an easy preparation, a high refractive index (∼2.5), and low optical losses. However, their technological processing is restricted, and hence, their application in integrated optics is limited. To overcome this issue, the incorporation of colloidal QDs in polymers is found to be a more suitable approach [5], [8]. Furthermore, polymers are cheap, flexible, and easily processed into films on several substrates, and can be micro- and nano-patterned by UV and e-beam lithography [9], respectively. In fact, the incorporation of colloidal QDs in polymers can be used for multiple applications: plasmonics [10], OLEDs [11], light amplification [12], and sensors [13]. Among others, PMMA and SU-8 resists are appropriate materials to fabricate integrated waveguides due to their high transparency above 400 nm and relatively high refractive index (∼1.5) [14], [15]. In [14], CdSe was incorporated in PMMA obtaining the optimal conditions for waveguiding, and results were extended to other kind of colloidal QDs (CdTe, CdS, and PbS) in [15], where also the emission wavelength tuning was shown by changing the base material without modifying the waveguide fabrication conditions. In this previous work, ridge waveguides based on SU-8 containing QDs were fabricated by using UV photolithography. Therefore, QD-polymer nanocomposites are excellent candidates to be the core of active waveguides not only for amplification purposes but also for displays [16] and sensing [17]. Moreover, two or three different types of QDs can be incorporated in the same waveguide to allow the transmission of several wavelengths [14], [15]. In this way, the waveguided photoluminescence (PL) by the QDs exhibits a broad spectrum, being it possible to obtain white light at the output of the structure with an appropriate selection of the QDs and their relative concentrations. White light emission has been demonstrated in OLEDs [18], by mixing CdSe of different sizes [19], changing the Se:S ratio in CdSeS nanocrystals [20] or using trap states in CdS and onion-like core-shell nanocrystals [21]. In addition, the pursuit of Cd-based QDs provides avenue for generation of visible light sources on Silicon template. It is important to note that the high efficiency visible light emitters had been primarily pursued by using InGaN-based polar quantum wells [22], semi/nonpolar QWs [23], [24], and new materials (i.e., dilute-As GaNAs) [25] for solid state lighting emitters. Recent works on the integration of III–V semiconductors on Silicon platform had also been reported [26].

In this paper, waveguides fabricated by the dispersion of CdS, CdSe, and CdTe in PMMA are studied by using the variable stripe method [27]. This pumping method allows an easy coupling of the light and gives information of the gain and losses of each waveguide. First, a study of the gain and losses as a function of the concentration of CdSe QDs in PMMA has been developed. Then, these results were extrapolated to CdTe and CdS QDs. Finally, the three types of QDs are mixed together in PMMA aiming to study the transfer of the light between them when PL propagates through the waveguide. This multicolor waveguiding can be applied for multiplexing applications. For example, it would be useful for sensing [17] or can be extended to QDs with emission in IR (PbS or PbSe) [15] to use it in telecommunications. As an useful application, we demonstrate that is possible to tune any waveguided color by formulating the nanocomposite with an appropriate concentration of three primary QD colors, to achieve particularly white light.

2. Experiment

2.1. QD Synthesis

CdS, CdTe, and CdSe nanocrystals were synthesized by the procedure developed using oleic acid as capping agent [28]. Because the QDs have different composition and size, they show different optical transitions, as revealed by their absorbance and PL spectra (see Fig. 1). Exciton absorption peaks of CdS, CdTe, and CdSe are placed at 447, 537, and 580 nm, corresponding to QD radii of 4.5, 1.5, and 2.4 nm, respectively [29]. For wavelengths shorter than the exciton peak, the absorbance increases and several excited states are observed. For longer wavelengths, the absorbance decreases, and it is virtually zero 100 nm above the exciton peak. The PL spectra of the three QD colloids are represented by single Gaussians centered at 453, 560, and 620 nm. The exciton PL peak is slightly red-shifted with respect to the exciton absorption (Stokes shift), which originates from the QD size distribution and the energy splitting of the ground exciton states [30].

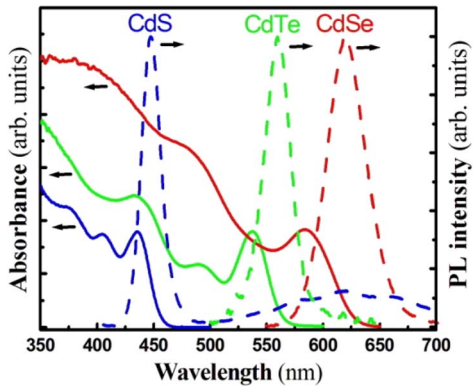

Fig. 1. Absorbance (left axis) and PL (right axis) of the colloidal CdS (blue), CdTe (green) and CdSe (red) used in this paper.

The full width at half-maximum (FWHM) is 20, 30, and 40 nm for CdS, CdTe, and CdSe QDs, respectively, which reflects the good monodispersity of the QDs. Finally, it is worth saying that CdS QDs exhibit a broad emission band centered at around 640 nm that is attributed to surface states [31], other than the dominant exciton ground state PL, as shown in Fig. 1 (blue dashed line).

2.2. Waveguide Fabrication

Once the colloidal QDs were synthesized, they were mixed with PMMA in order to fabricate the nanocomposite. For this purpose, both the polymer and the QDs were dissolved in toluene to achieve a good dispersion of the QDs in PMMA. We used a 9 wt.% PMMA in toluene. The concentration of nanoparticles in the polymer was chosen according to the results published in [14], where filling factors (ff) varying between 10^{-3} and 10^{-4} optimized the PL waveguiding. Then, planar waveguides were fabricated by spin coating the QD-PMMA solution on a SiO_2/Si substrate $(2\ \mu m\ SiO_2)$. The resulting film had a thickness of about 1 μm after two bakes at 80 °C and 150 °C for 2 min each. It is interesting to note that this thickness allows single mode propagation in the 450- to 650-nm range, as it has been deduced when the refractive index distributions were analyzed with the transfer matrix method [32]. Also, it is worth to say that the low index cladding layer is thick enough to isolate the propagation of the light from the polymer to the substrate. Finally, the edges of the samples were cleaved for end fire coupling purposes.

2.3. Optical Characterization

Absorption spectra of colloidal solutions were measured by using a Shimadzu UV-2501PC spectrophotometer. PL experiments were carried out by pumping the colloidal solution dropped on a glass slide with a 405-nm GaN laser. Then, the back-scattered PL signal was collected with a microscope objective to an optical fiber connected to a StellarNet EPP2000 spectrograph.

PL waveguiding in the structures was characterized by focusing the spot of the 405-nm laser in a stripe line on the top of the sample by using the experimental setup shown in Fig. 2. The power was fixed to 20 W/cm^2. In these conditions, the QDs are excited, and their PL is coupled to the waveguide and can be collected with a microscope objective focusing the light to a CCD camera or a fiber optics connected to a StellarNet EPP2000 spectrograph. The propagation of PL signal in waveguide follows the equation [27]:

$$\frac{dI_v(x)}{dx} = I_{SS} + (\Gamma \cdot g - \alpha) \cdot I_v(x) \quad (1)$$

where I_v is the intensity of the light, I_{SS} is the intensity of the spontaneous emission, g is the gain, Γ is the confinement factor of the waveguide mode, and α is the losses. The confinement factor

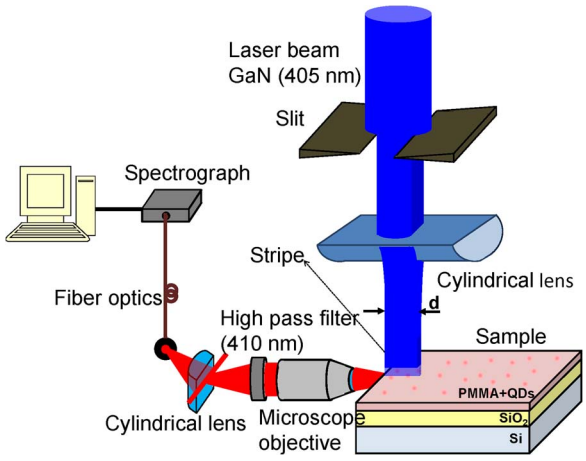

Fig. 2. Experimental setup.

can be calculated as the integrated power of the mode in the PMMA film with respect to the total integrated power of the mode and takes the values of 94.3%, 90.6%, and 85.6% at the wavelengths of 450, 550, and 580 nm respectively. Since, in the range of wavelengths used in this paper, there is not a strong variation, it will be considered into the value of g. Then, gain of the structure can be estimated by measuring the emission by the variable stripe length (VSL) method [27]. In order to avoid the influence of the Gaussian of the laser, a slit after the spot line was placed and kept the central 1.4 mm of the line. In these conditions, the gain of the structure can be calculated as

$$I(d) = \frac{I_{SS}}{g - \alpha} \cdot (e^{(g-\alpha)\cdot d} - 1). \tag{2}$$

In the same way, the attenuation of the waveguide can be characterized by keeping the length of the stripe constant and moving it away from the edge of the sample. Then, propagation losses can be fitted by approximating the dependence of the output intensity as a function of the distance between the stripe and the edge of the sample (x) with an exponential decrease

$$I(x) \propto e^{-\alpha \cdot x}. \tag{3}$$

3. Results and Discussion

3.1. CdSe-PMMA Waveguides

CdSe-PMMA waveguides were fabricated according to our previous work, using optimal QD filling factors (ff) for PL waveguiding between 10^{-4} and 10^{-3} [14]. In this paper, four different CdSe-PMMA samples were fabricated in order to investigate the influence of this factor in the gain and the losses of the films. Table 1 summarizes the samples studied in this section. The filling factor is calculated from the relative weight of PMMA and QDs in the final layer and the densities of each material. The effective refractive index of the nanocomposite is larger than that of the PMMA, given the high refractive index of the nanocrystals [14]. By using this parameter and the complex refractive indices of PMMA (n_{PMMA}) and CdSe (n_{QD}), the effective complex refractive index (n_{eff}) of the layer can be estimated using the Bruggeman approximation:

$$(1 - ff) \cdot \frac{n_{PMMA}^2 - n_{eff}^2}{n_{PMMA}^2 + 2 \cdot n_{eff}^2} + ff \cdot \frac{n_{QD} - n_{eff}^2}{n_{QD}^2 + 2 \cdot n_{eff}^2} = 0. \tag{4}$$

The dispersion curves of the PMMA and the real part of the CdSe were obtained from Nanocalc libraries. The imaginary part of the nanostructures was considered proportional to the absorbance

TABLE 1

Effective complex refractive index components and absorption coefficient as a function of *ff* in PMMA-CdSe samples

Sample	*ff*	n_{eff}'	n_{eff}''	α (cm^{-1})
A	$8.8\cdot 10^{-3}$	1.49893	10^{-3}	210
B	$4.4\cdot 10^{-3}$	1.49445	$6\cdot 10^{-4}$	126
C	$1.7\cdot 10^{-3}$	1.49172	$2\cdot 10^{-4}$	42
D	$4.5\cdot 10^{-4}$	1.49045	$6\cdot 10^{-5}$	13

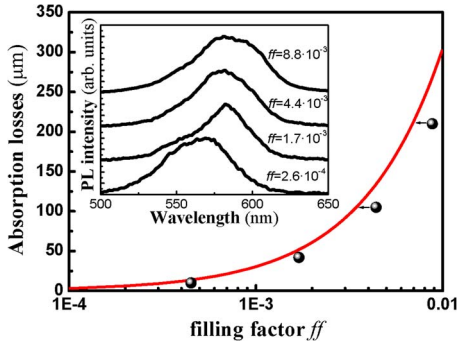

Fig. 3. Absorbance as a function of the filling factor. The inset shows the waveguided PL spectra for the concentrations listed in Table I.

curve depicted in Fig. 1 normalized to the absorption coefficient of the bulk CdSe at 350 nm. Table I summarizes the real part $(n_{eff'})$ and imaginary part (n''_{eff}) of the layers for each studied concentration at $\lambda = 580$ nm, where the exciton absorption peak is observed. Last column of the table indicates the absorption coefficient of the nancomposite at this wavelength using the relation $= (4 \cdot \tau \cdot n''_{eff})/\lambda$.

On the other hand, the absorption cross section of a single QD inside the polymer matrix is related to the absorption coefficient by [33]

$$C_{abs} = \frac{8 \cdot \pi^2 n_{PMMA}}{\lambda} \mathrm{Re}\{i \cdot \beta\} \tag{5}$$

where β is the polarizability of the QDs that is related to the radius of the QD (a) by:

$$\beta = \frac{n_{NQD}^2 - n_{PMMA}^2}{n_{NQD}^2 + 2 \cdot n_{PMMS}^2}\ a^3. \tag{6}$$

In this way, the absorption coefficient of the nanocomposite can be estimated by multiplying the absorption cross section [(5) and (6)] with the number of nanoparticles per unit volume, which can be calculated as a function of *ff*, as shown in Fig. 3 (red continuous line). The absorption coefficients found using this estimate in the four samples are very close to the ones calculated with the Bruggeman approach, as listed in Table I and shown in Fig. 3 (solid circles). As shown in Fig. 1, absorption strongly increases for wavelengths below the QD effective band gap. Then, the waveguide suffers from high attenuation losses at wavelengths close to the UV, but it can propagate the light for wavelengths above 600 nm [14]. For example, a light beam at 405 nm was attenuated more than 30 orders of magnitude by end fire coupling in a waveguide of 5-mm length and $ff = 10^{-3}$ [14]. On the contrary, it is possible to excite the QDs at this wavelength from the top

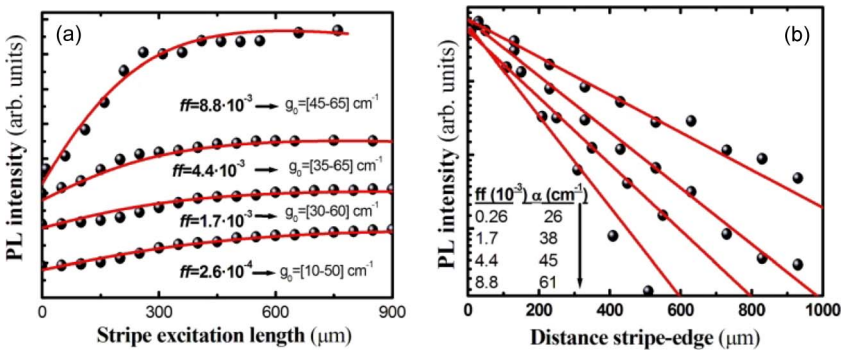

Fig. 4. (a) PL intensity as a function of the stripe excitation length for four different filling factors of CdSe in PMMA. (b) PL intensity as a function of the distance between the stripe and the edge of the sample for the same samples. The values of g_0 and α estimated and indicated in the figures.

surface by focusing into a stripe line as described in Section 2. The PL generated by pumped QDs can propagate through the waveguide, even if the overlap between absorption and emission curves (see Fig. 1) will limit the propagation of the waveguided PL. As long as the filling factor is increased the PL band becomes asymmetric due to that partial self-absorption of the PL by the QDs, as shown in the inset of Fig. 3, which is more important for higher filling factors.

Fig. 4(a) shows the dependence of the PL intensity as a function of the length of the stripe for samples listed in Table I (black solid circles). The signal increases significantly with the length of the stripe and reaches saturation for lengths between 300 and 900 μm, depending on the concentration. This behavior can be fitted considering a gain saturation function in (1) with the form

$$g = g_0 \cdot e^{-d/L} \tag{7}$$

where d is the stripe length, and g_0 and L are fitting parameters related to an initial gain and a propagation attenuation length characteristic of the gain saturation, most probably originated by Auger nonradiative recombination in the QDs [3], [10], [34]. This saturation is applied in this paper by introducing (7) in (1) and solving the differential equation by a Runge–Kutta algorithm. The result of the simulation is depicted in Fig. 4(a) (red continuous lines). Clearly, the model can fit accurately the data by using appropriate values for g_0 and L. In all cases, L can be ranged between 200 and 250 μm to get the best fittings. The value of g_0 obtained from the best fits tends to increase with *ff* due to the growing amount of QDs, as observed in Fig. 4(a). For low concentrations ($ff \sim 4.5 \cdot 10^{-4}$) g_0 reaches a value of 30 ± 20 cm^{-1} and increases up to 55 ± 10 cm^{-1}. The increment in g_0 results in the increase in the slope of the waveguided PL intensity curve, as observed in Fig. 4(a). On the other hand, more absorption losses are also expected by increasing *ff* due to the overlap between absorption and emission bands of QDs in PMMA, as observed in Fig. 4(b) (black solid circles). These experimental losses fitted with the exponential decay given by (3) increase from 26 to 61 cm^{-1} for samples D to A [red continuous lines in Fig. 4(b)]. For low *ff* values, the loss coefficient is close to the absorption coefficient estimated in the nanocomposite (data symbols and continuous curve in Fig. 3), but this is not the case for high *ff* values, probably due to an overestimation of the concentration. In all cases, losses are very similar to values deduced for g_0; in consequence, there is no net gain in the waveguides and amplification will be not possible. Indeed, it is worth saying that all samples show a linear dependence with pumping power with no variation in the spectrum lineshape [14].

3.2. CdTe-PMMA and CdS-PMMA Waveguides

Waveguides based on CdS and CdTe QDs in PMMA were fabricated and characterized using the same procedure explained in the last section. In this case, low *ff* values have been used in order to

TABLE 2

Effective complex refractive index components and absorption coefficient for two low *ff* samples made of PMMA-CdS and PMMA-CdTe

Sample	QD	*ff*	n_{eff}'	n_{eff}''	α (cm^{-1})
E	CdS (450 nm)	10^{-4}	1.4991	$8 \cdot 10^{-6}$	2
F	CdTe (540 nm)	$4 \cdot 10^{-4}$	1.4925	$1.7 \cdot 10^{-4}$	14

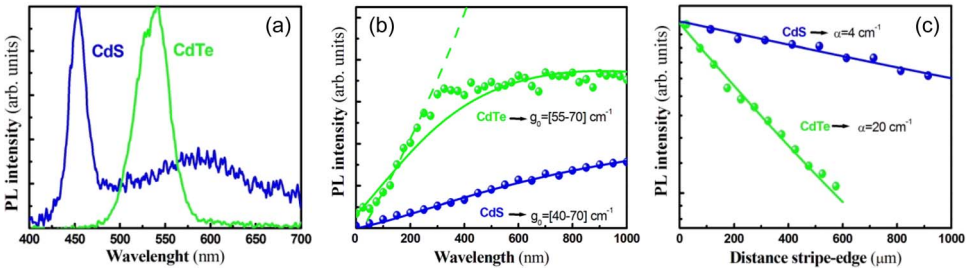

Fig. 5. (a) Waveguided PL spectra in CdS-PMMA (blue curve) and CdTe-PMMA (green curve) waveguides; (b) PL intensity as a function of the stripe excitation length; (c) PL intensity as a function of the distance between the stripe and the edge of the sample. Green and blue colors refers to CdTe-PMMA and CdS-PMMA waveguides, respectively. Green dotted line stands for a fit to equation (2) without a gain saturation function. The values of the best fitting parameters g_0 and α are indicated in the figures.

minimize self-absorption of the QDs. Table 2 lists the samples and the complex refractive indices calculated with the Bruggeman method. The absorption coefficient at the exciton peaks (450 and 540 nm for CdS and CdTe QDs, respectively) were 2 and 14 cm^{-1} for samples E and F, respectively. Again, these values are close to the ones obtained using (5) and (6).

Fig. 5 shows PL spectra (blue and green continuous curves for CdS and CdTe samples, respectively) (a) and characterization of gain (b) and losses (c) by the VSL method (blue and green solid circles for CdS and CdTe samples, respectively). The PL peak in the CdS-PMMA waveguides is centered at 450 nm, and its linewidth is about 15 nm, even if a broad and weak PL band is measured at 640 nm that is attributed to carrier recombination through surface states. The PL emission band in the CdTe-PMMA waveguides is centered at 540 nm and has a linewidth of 35 nm. The simulation using the model explained in Section 3 (blue and green continuous lines) reproduces quite well the experimental results (data symbols). Again, the Auger attenuation length L found to obtain the best fits is in the range of 200–250 μm. For these values of L, the best fitting curves were obtained with g_0 equal to 55 ± 15 and 63 ± 8 cm^{-1} in samples E (CdS-PMMA) and F (CdTe-PMMA), respectively. Regarding losses, the best fitting curves yield $\alpha = 4$ and 20 cm^{-1} for CdS and CdTe QDs, respectively, as shown in Fig. 5(c) (blue and green straight lines), which are very close to the ones listed in Table I. Such a reduced absorption loss in the case of the CdS-PMMA waveguide with respect to the case of CdTe- and CdSe-PMMA waveguides with similar concentrations can be explained by the fact that the size of CdS QDs in the polymer is practically double to that of CdSe QDs, and hence, a similar difference in the quantity of QDs in the nanocomposite is expected. Finally, we strengthen that net gain is obtained for a pumping stripe beam shorter than the Auger attenuation length in CdS- and CdTe-PMMA waveguides. Finally, it is interesting to note that net gain can be obtained in the CdTe-PMMA waveguide when the length of the pumping stripe beam is shorter than the Auger attenuation length. Indeed, the first 300 nm of the curve can be fitted through (2) using a net gain of around 10 cm^{-1} [see dashed line in Fig. 5(b)].

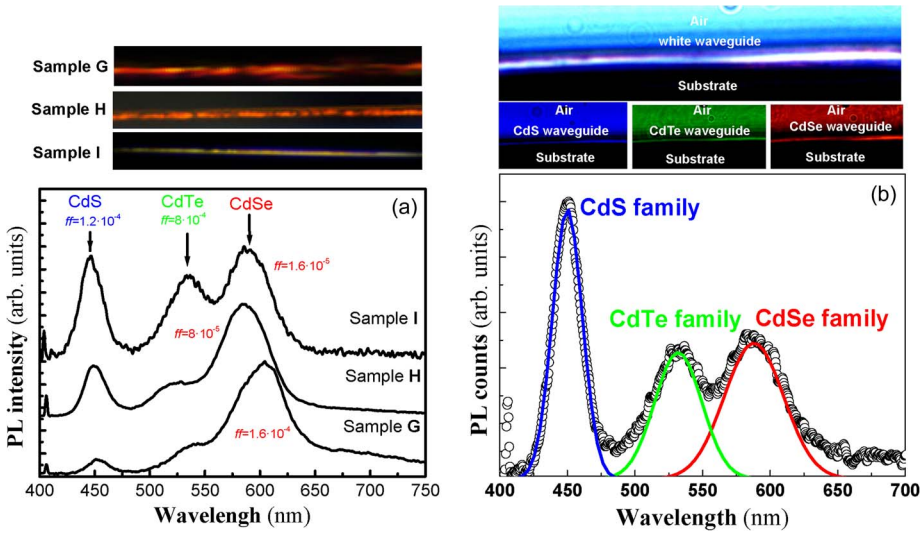

Fig. 6. (a) Waveguided PL spectra in samples G, H and I. (b) Waveguided PL spectra in sample J. Top panels show a photographs of the waveguided PL.

3.3. Multicolor Waveguiding

If more than one type of QDs is dispersed in the same polymer, the resulting film shows a broad waveguided PL spectrum, as a convolution of the different QD optical transitions [14], [15]. In this way, the light at the output of the integrated optic structure can be engineered by controlling the concentration of each type of nanoparticles embedded in the polymer. Fig. 6(a) shows the waveguided PL spectra measured in samples G, H, and I. In these samples, the *ff* values of CdS and CdTe QDs in PMMA were fixed to $1.2 \cdot 10^{-3}$ and $3 \cdot 10^{-4}$, respectively, whereas the concentration of CdSe QDs was varied: $ff = 1.8 \cdot 10^{-4}$ (sample G), $ff = 9 \cdot 10^{-4}$ (sample H), and $ff = 1.8 \cdot 10^{-5}$ (sample I). We observe that the relative intensities between the different components changes among the three samples. As expected, the PL band associated to CdSe QDs (PL peak at 580–600 nm) becomes more important as long as its concentration is increased into the film. However, the ratio between the PL components associated to CdTe (450 nm) and CdS (540 nm) QDs unexpectedly decreases with the presence of CdSe, which can be attributed to partial light absorption by some of the QD ensembles of light emitted by the others, as will be explained below. As a consequence, the color of the waveguided PL in the multiple-QD nanocomposite changes from red to yellow from sample G to I, respectively. The top panels of Fig. 6(a) show the CCD photographs of the PL at the end of G, H, and I waveguides. Therefore, the waveguided color can be tuned by an appropriate combination (*ff* of the QDs) of the three different ensembles of QDs, and hence, white light at the output of the structure can be also engineered. White light emission has already been demonstrated in OLEDs incorporating colloidal QDs [35] or dyes [36], which will be important to define future low consuming displays. The definition of the white light at the exit of the waveguide will be achieved by obtaining a similar integrated intensity for the pure red, green, and blue components [37]. By extrapolating this condition to our multiple-QD (CdS, CdTe, and CdSe) nanocomposite and taking into account results in Fig. 6(a) for samples G–I, waveguided white light can be achieved, as shown in Fig. 6(b) for sample J. The waveguided PL spectrum is clearly composed by the same three PL components centered at 450 nm (CdS), 530 nm (CdTe), and 590 nm (CdS). On the top panel of Fig. 6(b), a CCD photograph shows the waveguided white color as a result of the three PL band convolutions.

As demonstrated in Fig. 6(a), the waveguided PL spectrum obtained by the combination of several QD families is influenced not only by the emission of the individual QD ensembles (without interaction) but also by the partial light absorption by some of the QD ensembles (CdTe and CdSe,

TABLE 3

Filling factor and absorption coefficient at the characteristic peak exciton wavelength in several multi-QD CdS-CdTe-CdSe/PMMA samples

Sample	CdS *ff*	CdTe *ff*	CdSe *ff*	α (cm^{-1})		
				450 nm	540 nm	580 nm
G	$1.2 \cdot 10^{-3}$	$3 \cdot 10^{-4}$	$1.6 \cdot 10^{-4}$	52	34	5
H	$1.2 \cdot 10^{-3}$	$3 \cdot 10^{-4}$	$9 \cdot 10^{-5}$	45	32	2
I	$1.2 \cdot 10^{-3}$	$3 \cdot 10^{-4}$	$1.6 \cdot 10^{-5}$	40	31	1
J	$2.4 \cdot 10^{-3}$	$3 \cdot 10^{-4}$	$1.6 \cdot 10^{-5}$	40	31	1

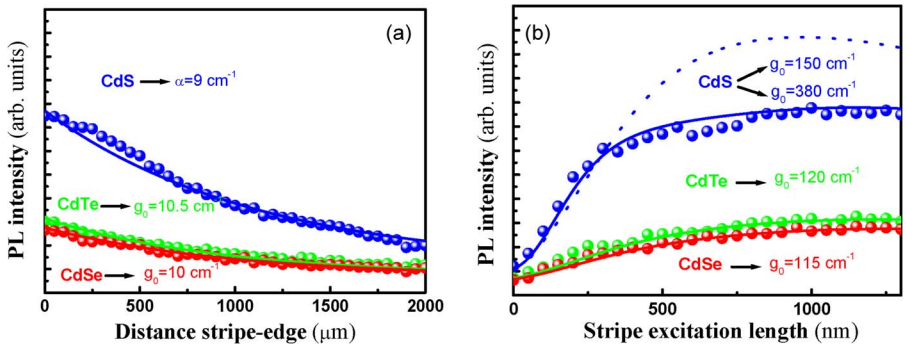

Fig. 7. (a) PL intensity as a function of the stripe excitation in sample J. (b) PL intensity as a function of the distance between the line and the edge of the sample. Blue, green and red colors refer to CdS, CdTe, and CdSe families.

characterized by optical transitions at longer wavelengths) of light emitted by others (CdS and CdTe, characterized by optical transitions at shorter wavelengths). This effect is originated by the overlap between the absorption and PL emission curves, as shown in Fig. 1. Then, the CdSe QD ensemble is the only one that gain intensity from both CdS and CdTe QDs, whereas the CdS QD ensemble is the only one that loses emitted photons toward CdTe and CdSe QDs; at the middle, the CdTe QD ensemble gains photons from CdS QDs and loses toward CdSe QDs. This partial absorption effect of emitted light propagating in the waveguide can be calculated using the absorption cross sections (σ) and the number of QDs per unit volume (N) of each material

$$\alpha(\lambda) = \sigma_{\text{cdSe}}(\lambda) \cdot \text{N}_{\text{CdSe}} + \sigma_{\text{CdTe}}(\lambda) \cdot \text{N}_{\text{CdTe}} + \sigma_{\text{CdS}}(\lambda) \cdot \text{N}_{\text{CdS}}. \quad (8)$$

Given the low value of *ff* used in samples G–J (see Table 3), the real part of the refractive index can be approximated to that of PMMA. Table 3 summarizes the absorption coefficients calculated at the wavelengths of 450 (CdS QDs), 540 (CdTe QDs), and 580 (CdSe QDs) nm. According to these calculations, it is expected that the CdS band will be strongly attenuated through the sample. However, when VSL characterization was carried out in this set of samples, the three bands showed similar losses of about 10 cm^{-1} for all PL components (by filtering the whole emission band), as shown in Fig. 7(a). Moreover, CdSe and CdTe PL components had a similar dependence with the length of the stripe [red and green data symbols in Fig. 7(b)], whereas the CdS PL component exhibited a higher gain behavior [blue data symbols in Fig. 7(b)] indicating that another mechanism of photon redistribution among the different QD families could be present.

The waveguided PL components associated to CdSe and CdTe QD families exhibit a similar intensity growth with values of g_0 around 120 cm^{-1} [red and green continuous lines in Fig. 7(b) are the best fitting curves] may be due to the additional photon transfer by absorption of emitted light by

CdS QDs in sample J. In fact, the best fit [blue continuous line in Fig. 7(b)] to the experimental intensity growth measured for CdS QDs is obtained for g_0 and L within the intervals 150–380 cm^{-1} and 70–100 μm, respectively. These values for L are smaller than those obtained above in nanocomposites formed by a single QD family (where L was found between 200 and 250 μm) and indicate a faster saturation in the multi-QD structure [see dotted line in Fig. 7(b) that has been calculated with $L = 200$ μm for a better comparison]. Therefore, results obtained by the VSL method suggest the presence of an extra mechanism responsible of photon redistribution among the different QD ensembles. As noted above in the case of single-QD-loaded CdTe-PMMA samples, the fast slope of the waveguided PL for the CdS-QD component is smaller than the Auger attenuation length, and hence, net gain could be possible within the first 300 μm of the stripe excitation length. Indeed, this first zone of the curve [blue symbols in Fig. 7(b)] can be fitted through (2) using a net gain of about 5 cm^{-1}.

A possibility to explain that extra mechanism can be found in the analogy to a system constituted by different fluorophores where Förster resonant energy transfer occurs [38]. This process consists in the nonradiative transfer of the excitation energy from a donor (absorbing fluorophor) to an acceptor (emitting fluorophor) due to a dipole–dipole interaction, which can be activated if the overlap between the acceptor absorption and the donor fluorescence spectra is appreciable and the maximum interdistance of species is around 50 Å [39], [40]. The first condition is fulfilled in our multiple-QD nanocomposite, as was explained above. Concerning the distances between nanoparticles, the number of QDs per μm^3 of each family can be estimated dividing the *ff* by the volume of the nanostructures (considered spheres of radius *a*)

$$N = ff \cdot \frac{1\mu m^s}{\frac{4}{3}\pi a^s}. \tag{9}$$

The number of QDs in G–J samples results in the order of $3-6 \cdot 10^3$, 10^4 and $3-30 \cdot 10^2$ for CdS, CdTe, and CdSe depending on the sample. If one assumes that the nanoparticles are homogeneously distributed over the volume of the film, the number of them along one direction would be the third root of those values. This number can be of the order of 15, 28, and 7 for CdS, CdTe, and CdSe, respectively, in total about 50 nanoparticles/μm, which means an average interdistance $\approx$20 nm, by considering the minimum QD concentrations (14 nm in the case of the maximum values). These distances are too high to justify the Förster energy transfer mechanism. However, a perfect homogeneous and random distribution in QD-polymer nanocomposites is far from the real situation, where nanoparticle aggregation normally takes place. In fact, this is the mechanism explaining electroluminescence in QD-polymer nanocomposites via field-driven ionization [41]. That aggrupation of several nanoparticles can lead to QD interdistances as low as 1 nm (the size of the ligand) and hence allowing the Förster energy transfer mechanism inside the aggregates. Furthermore, the highest efficiency of that energy transfer mechanism is expected between CdS and CdTe QDs, given the larger overlap between their absorption (CdS) and PL (CdTe) spectra and their highest concentration.

In summary, when the waveguide is pumped at 405 nm, emitted photons by CdS QDs can be partially reabsorbed by CdTe and CdSe QDs, other than the Förster energy transfer, explaining higher g_0 values than using nanocomposites with a single QD ensemble. Concerning the losses shown in Fig. 7(b), the fact that the three families show similar values indicates that in these samples where the concentration of nanoparticles is not too big, the attenuation is dominated by scattering in the polymer or the diffraction of the light in the stripe [42]. In addition, if aggregation of several QDs takes place, this will reduce the average homogeneous distribution of QDs from numbers estimated above and hence lead to smaller absorption coefficient values. This can be also the reason of the observed deviation between losses deduced in samples A–D by the VSL method [see Fig. 4(b)] and absorption coefficient (see Fig. 3) noted above when increasing the content of CdSe QDs.

4. Conclusion

In this paper, the propagation of emitted photons by CdS, CdTe, and CdSe QDs has been studied using the VSL method to pump active waveguides made of PMMA doped with them, separately. A simple model has been used to explain the saturation of the gain through an Auger attenuation length. In the second part of the paper, several waveguides containing the three different QDs dispersed in PMMA have been fabricated and studied by spectroscopy and by the VSL method. From one side, the appropriate relative content of the three sets of QDs can be adjusted to obtain a given color at the exit of the waveguide, particularly demonstrated to get white light. On the other side, reabsorption and photon redistribution among QDs (by Förster energy transfer) effects should be taken into account for that relative content adjusts. Finally, Förster energy transfer can be also the reason that higher initial gain and smaller losses are deduced in these multi-QD waveguides as compared with the case of single-QD ones. This photon engineering can be translated to other applications as QD-LEDs and QD-displays, among the most important ones.

References

[1] V. I. Klimov, "Nanocrystal quantum dots: From fundamental photophysics to multicolor lasing," *Los Alamos Sci.*, vol. 28, no. 60, pp. 214–220, Sep. 2003.

[2] P. Alivisatos, "Perspectives on the physical chemistry of semiconductor nanocrystals," *J. Phys. Chem.*, vol. 100, no. 31, pp. 13 226–13 239, Aug. 1996.

[3] V. I. Klimov, A. A. Mikhailovsky, S. Xu, A. Malko, J. A. Hollingsworth, C. A. Leatherdale, H. J. Eisler, and M. G. Bawendi, "Optical gain and stimulated emission in nanocrystal quantum dots," *Science*, vol. 290, no. 5490, pp. 314–317, Oct. 2000.

[4] Y. Chan, J. S. Steckel, P. T. Snee, J. M. Caruge, J. M. Hodgkiss, D. G. Nocera, and M. G. Bawendi, "Blue semiconductor nanocrystal laser," *Appl. Phys. Lett.*, vol. 86, no. 7, pp. 073102-1–073102-3, Feb. 2005.

[5] C. Dand, J. Lee, C. Breen, J. S. Steckel, S. Coe-Sullivan, and A. Nurmikko, "Red, green and blue lasing enabled by single-exciton gain in colloidal quantum dot films," *Nature Nanotechnol.*, vol. 7, no. 5, pp. 335–339, May 2012.

[6] N. Tomczak, D. Janczeuski, M. Han, and G. Julius Vancson, "Designer polymer-quantum dot architectures," *Progr. Polym. Sci.*, vol. 34, no. 5, pp. 393–430, May 2009.

[7] J. Jasieniak, J. Pacifico, R. Signorini, A. Chiasera, M. Ferrari, A. Martucci, and P. Mulvaney, "Luminescence and amplified stimulated emission in CdSe-ZnS-nanocrystal-doped TiO_2 and ZrO_2 waveguides," *Adv. Funct. Mater.*, vol. 17, no. 10, pp. 1654–1662, Jul. 2007.

[8] L. Pang, K. Tetz, Y. Shen, C. H. Chen, and Y. J. Fainman, "Photosensitive quantum dot composites and their applications in optical structures," *J. Vac. Sci. Technol. B, Microelectron. Nanom. Struct.*, vol. 23, no. 11, pp. 2413–2419, Nov. 2005.

[9] M. A. Uddin and H. P. Chan, "Materials and process optimization in the reliable fabrication of polymer photonic devices," *J. Optoelectron. Adv. Mater.*, vol. 10, no. 1, pp. 1–17, Jan. 2008.

[10] J. Grandidier, G. Colas des Francs, S. Massenot, A. Bouhelier, L. Markey, J. C. Weeber, C. Finot, and A. Dereux, "Gain-assisted propagation in a plasmonic waveguide at telecom wavelength," *Nano Lett.*, vol. 9, no. 8, pp. 2935–2939, Aug. 2009.

[11] A. L. Rogach, N. Gaponik, J. M. Lupton, C. Bertoni, D. E. Gallardo, S. Dunn, N. Li Pira, M. Paderi, P. Repetto, S. G. Romanov, C. O'Dwyer, C. M. Sotomayor Torres, and A. Eychmüller, "Light-emitting diodes with semiconductor nanocrystals," *Angew. Chem. Int. Ed.*, vol. 47, no. 35, pp. 6538–6549, Aug. 2008.

[12] T. N. Smirnova, O. V. Sakhno, P. V. Yezhov, L. M. Kokhtych, L. M. Goldenberg, and J. Stumpe, "Amplified spontaneous emission in polymer-CdSe/ZnS-nanocrystal DFB structures produced by the holographic method," *Nanotechnology*, vol. 20, no. 24, p. 245 707, Jun. 2009.

[13] P. Jorge, M. A. Martins, T. Trindade, J. L. Santos, and F. Faramarz, "Optical fiber sensing using quantum dots," *Sensors*, vol. 7, no. 12, pp. 3489–3534, Dec. 2007.

[14] I. Suárez, H. Gordillo, R. Abargues, S. Albert, and J. Martínez-Pastor, "Photoluminescence waveguiding in CdSe and CdTe QDs-PMMA nanocomposite films," *Nanotechnol.*, vol. 22, no. 43, p. 435202, Oct. 2011.

[15] H. Gordillo, I. Suárez, R. Abargues, P. J. Rodríguez-Cantó, S. Albert, and J. P. Martínez-Pastor, "Polymer/QDs nanocomposites for wave-guiding applications," *J. Nanomater.*, vol. 2012, no. 4, pp. 960201-1–960201-9, Apr. 2012.

[16] J. N. Kuo, H. W. Wu, and G. B. Lee, "Optical projection display systems integrated with three-color-mixing waveguides and grating-light-valve devices," *Opt. Exp.*, vol. 14, no. 15, pp. 6844–6850, Jul. 2006.

[17] A. Bueno, I. Suárez, R. Abargues, S. Sales, and J. P. Martínez-Pastor, "Temperature sensor based on colloidal quantum dots-PMMA nanocomposite waveguides," *IEEE Sensors J.*, vol. 12, no. 10, pp. 3069–3074, Oct. 2012.

[18] J. Lee, V. C. Sundar, J. R. Heine, M. G. Bawendi, and K. F. Jensen, "Full color emission from II-VI semiconductor quantum dot-polymer composites," *Adv. Mater.*, vol. 12, no. 15, pp. 1100–1102, Aug. 2000.

[19] X. Liu, Y. Jiang, C. Wang, S. Li, X. Lan, and Y. Chen, "White-light-emitting CdSe quantum dots with 'magic size' via one-pot synthesis approach," *Phys. Stat. Sol. (A)*, vol. 207, no. 11, pp. 2472–2477, Nov. 2010.

[20] M. Ali, S. Chattopadhayay, A. Nag, A. Kumar, S. Sapra, S. Chakraborty, and D. Sarna, "White-light emission from a blend of CdSeS nanocrystals of different Se:S ratio," *Nanotechnology*, vol. 18, no. 7, p. 075401, Feb. 2007.

[21] S. Sapra, S. Mayilo, T. A. Klar, A. L. Rogach, and J. Feldmann, "Bright white-light emission from semiconductor nanocrystals: By chance and by design," *Adv. Mater.*, vol. 19, no. 4, pp. 569–572, Feb. 2007.
[22] H. Zhao, G. Liu, J. Zhang, J. D. Poplawsky, V. Dierolf, and N. Tansu, "Approaches for high internal quantum efficiency green InGaN light-emitting diodes with large overlap quantum wells," *Opt. Exp.*, vol. 19, no. S4, pp. A991–A1007, Jul. 2011.
[23] R. M. Farrell, E. C. Young, S. P. DenBaars, and J. S. Speck, "Materials and growth issues for high-performance nonpolar and semipolar light-emitting devices," *Semicond. Sci. Technol.*, vol. 27, no. 2, pp. 024001-1–024001-14, Feb. 2012.
[24] D. F. Feezell, J. S. Speck, S. P. DenBaars, and S. Nakamura, "Semipolar InGaN/GaN light-emitting diodes for high-efficiency solid-state lighting," *J. Display Technol.*, vol. 9, no. 4, pp. 190–198, Apr. 2013.
[25] C. K. Tan, J. Zhang, X. H. Li, G. Liu, B. O. Tayo, and N. Tansu, "First-principle electronic properties of dilute-As GaNAs alloy for visible light emitters," *J. Display Technol.*, vol. 9, no. 4, pp. 272–279, Apr. 2013.
[26] D. Liang and J. E. Bowers, "Recent progress in lasers on silicon," *Nature Photon.*, vol. 4, no. 8, pp. 511–517, Aug. 2011.
[27] L. Dal Negro, P. Bettotti, M. Cazzanelli, D. Pacifi, and L. Pavesi, "Applicability conditions and experimental analysis of the variable stripe length method for gain measurements," *Opt. Commun.*, vol. 229, no. 1–6, pp. 337–348, Jan. 2004.
[28] W. W. Yu and X. Peng, "Formation of high-quality CdS and other II-VI semiconductor nanocrystals in noncoordinating solvents: Tunable reactivity of monomers," *Angew. Chem. Int. Ed.*, vol. 41, no. 13, pp. 2368–2371, Jul. 2002.
[29] W. W. Yu, L. Qu, W. Guo, and X. Peng, "Experimental determination of the extinction coefficient of CdTe, CdSe and CdS nanocrystals," *Chem. Mater.*, vol. 15, no. 14, pp. 2854–2860, Jul. 2003.
[30] J. E. Boercker, E. M. Clifton, J. G. Tischler, E. E. Foos, T. J. Zega, M. E. Twigg, and R. M. Stroud, "Size and temperature dependence of band-edge excitons in PbSe nanowires," *J. Phys. Chem. Lett.*, vol. 2, no. 6, pp. 527–531, Mar. 2011.
[31] L. Hu, H. wu, L. Du, H. Ge, X. Chen, and N. Dai, "The effect of annealing and photoactivation on the optical transitions of band-band and surface trap states of colloidal quantum dots in PMMA," *Nanotechnology*, vol. 22, no. 12, pp. 125202-1–125202-6, Mar. 2011.
[32] G. Lifante, *Integrated Photonics. Fundamentals*. Hoboken, NJ, USA: Wiley, 2003.
[33] C. A. Leatherdale, W. K. Woo, F. V. Mikulec, and M. G. Bawendi, "On the absorption cross section of CdSe nanocrystal quantum dots," *J. Phys. Chem. B*, vol. 106, no. 31, pp. 7616–7622, Aug. 2002.
[34] J. J. Jasieniak, I. Fortunati, S. Gardin, R. Signorini, R. Bozio, A. Martucci, and P. Mulvaney, "Highly efficient stimulated emission from CdSe-CdS-ZnS quantum dot doped waveguides with two-photon infrared optical pumping," *Adv. Mater.*, vol. 20, no. 1, pp. 69–73, Jan. 2008.
[35] Y. Liao, G. Xing, N. Mishra, T. C. Sum, and Y. Chan, "Low threshold, amplified spontaneous emission from core-seeded semiconductor nanotetrapods incorporated into a sol-gel matrix," *Adv. Mater.*, vol. 24, no. 23, pp. OP159–OP164, Jun. 2012.
[36] A. A. Shoustikov, Y. You, and M. E. Thompson, "Electroluminescence color tuning by dye doping in organic light-emitting diodes," *IEEE J. Sel. Topics Quantum Electron.*, vol. 4, no. 1, pp. 3–13, Jan./Feb. 1998.
[37] M. C. Gather, Köhnen, and K. Meerholz, "White organic light-emitting diodes," *Adv. Mater.*, vol. 23, no. 2, pp. 233–248, Jan. 2011.
[38] A. L. Rogach, T. A. Klar, J. M. Lupton, A. Meijerink, and J. Feldmann, "Energy transfer with semiconductor nanocrystals," *J. Mater. Chem.*, vol. 19, no. 9, pp. 1208–1221, Nov. 2009.
[39] Y. Li, A. Rizzo, M. Mazzeo, L. Carbone, L. Manna, R. Cingolani, and G. Gigli, "White organic light-emitting devices with CdSe/ZnS quantum dots as a red emitter," *J. Appl. Phys.*, vol. 97, no. 11, pp. 113501-1–113501-4, Jun. 2005.
[40] A. Rizzo, M. Mazzeo, M. Biasiucci, R. Cingolani, and G. Gigli, "White electroluminescence from a microcontact-printing-deposited CdSe/ZnS colloidal quantum-dot monolayer†," *Small*, vol. 4, no. 12, pp. 2143–2147, Dec. 2008.
[41] V. Wood, M. J. Panzer, D. Bozyigit, Y. Shirasaki, I. Rousseau, S. Geyer, M. G. Bawendi, and V. Bulovic, "Electroluminescence from nanoscale materials via field-driven ionization," *Nano Lett.*, vol. 11, no. 7, pp. 2927–2932, Jul. 2011.
[42] J. Valenta, I. Pelant, and J. Linnros, "Waveguiding effects in the measurement of optical gain in a layer of Si nanocrystals," *Appl. Phys. Lett.*, vol. 81, no. 8, pp. 1396–1398, Aug. 2002.